

In situ tailoring solid electrolyte interphase of three-dimensional Li metal electrode for enhanced Coulombic efficiency

Jiangpeng Wang¹, FENG LANG¹, and Quan Li¹

¹The Chinese University of Hong Kong

February 7, 2023

Abstract

Although three-dimensional (3D) host is effective in restricting Li dendrite growth, problems associated with the unstable electrode/electrolyte interphase becomes more severe due to increased interfacial area that is intrinsic of the 3D structures, being a major cause for the low Coulombic efficiency. While building a desirable solid electrolyte interphase (SEI) serves as an effective solution to improve the electrode/electrolyte interfacial stability, the 3D nature of the electrode makes the task challenging. Herein, we demonstrated the in-situ formation of SEI on chemically/structurally modified carbon cloth that is used as the 3D host. We shown that ZnS/ZnO nanotube arrays uniformly grown on the carbon cloth served as precursors for the in-situ formation of Li₂S/Li₂O/LiZn containing artificial SEI. While Li₂S and Li₂O are preferred components in SEI, Zn functions as lithiophilic site that guides the uniform lithium deposition. The present work shed light on effective design strategies for SEI formation on 3D electrode host with controllable SEI composition.

INTRODUCTION

Lithium metal is a promising anode candidate for developing high-energy-density Li-based batteries due to its ultrahigh specific capacity (3860 mA h g⁻¹) and low redox potential (-3.040 V versus the standard hydrogen electrode).^[1-3] Unfortunately, uncontrollable lithium dendrite growth during the electrochemical process and the unstable electrode/electrolyte interface result in poor cycle life, low Coulombic efficiency (CE), and even explosion.^[4-6]

Among various strategies attempted to tackle the aforementioned problems,^[7-12] constructing a three-dimensional (3D) current collector is an efficient method to mitigate dendrite growth as the 3D configuration with a high specific surface area and the porous structure can reduce the local current density and accommodate the volume change upon repeated stripping/plating.^[13,14] A number of successful demonstrations of uniform Li deposition by adopting the 3D strategy can be found in the literature, such as porous metal-based foams and 3D carbon-based frameworks.^[15-18] However, the high specific surface area of a 3D host is double-bladed, as it also leads to an increased interfacial reaction between the Li metal and electrolyte, making the already unstable interface (between Li and existing electrolytes) worse, and serving as a major contributor to the low Coulombic efficiency commonly associated with the 3D configuration.^[19,20] To improve the CE, constructing artificial solid-electrolyte interphase (SEI) to reduce the irreversible reaction between electrolyte and lithium metal is a commonly adopted method.^[21,22] To date, most of the artificial SEI layers are constructed either on lithium metal or planar current collectors,^[23-25] although interfacial stability is a particularly critical issue in the 3D configuration and building an efficient artificial SEI layer on the 3D host may represent a most promising solution to simultaneously achieving long cycle stability and high CE. Recently, a couple of attempts have been made to build SEI on 3D electrode hosts. For example, Zhai et al. designed a 3D g-C₃N₄/G/g-C₃N₄ architecture, and a high average CE (99.1%) was achieved for 500 cycles at 1 mA cm⁻²/1 mA h cm⁻².^[26] Liu et al. reported a LiBr-LiF-rich SEI on the surface of 3D sponge nickel, and the assembled cell exhibited a good cycle life (over 800 cycles at 1 mA cm⁻²/1 mA h cm⁻²).^[27] Carbon cloth

is an important 3D substrate in constructing composite lithium metal anode because of its good chemical stability, excellent mechanical performance, and electrical conductivity. Its 3D architecture has been found to effectively reduce the local current density and accommodate lithium. However, the commercial carbon cloth is lithiophobic, and the existing modification strategies mainly focused on functional groups grafting (-C=O, -COOH), heteroatom doping (N/S/P co-doping, O doping), and lithiophilic material decorating.^[28-31] Most recently, Cao et al. reported CoSe₂ anchored carbon fiber cloth to enhance lithiophilicity by forming Co/Li₂Se, and the system exhibited excellent cycle performance.^[32]

Herein, we demonstrated uniform surface decoration of carbon cloth by ZnS/ZnO nanotubes (ZSONT/CC), serving as a multifunctional skeleton to host lithium metal for anode applications. The formed nanotube uniformly covers the entire surface of the individual carbon fiber. Most importantly, during the electrochemical pre-lithiation process, ZnS and ZnO serve as precursors for in situ generations of SEI containing Li₂S, Li₂O, and LiZn, which materials are most desirable for SEI functionality. More specifically, it is known that Li-Zn alloy enhances the affinity of the 3D host to lithium and thus guides the uniform lithium deposition.^[33] Li₂S possesses a low Li diffusion energy barrier (0.28 eV) and a high ionic conductivity (10⁻⁵ S cm⁻¹), which enable fast Li⁺ transport kinetics.^[34] Li₂O has an affinity for lithium and can also reduce the elastic strain energy between the plated lithium and the substrate because of the lower crystalline mismatch.^[35] As a result, the Li/ZSONT/CC half-cell can last for 700 hours at 4 mA cm⁻² / 4 mA h cm⁻². A stable CE of 99.2% is achieved over 400 cycles at 1 mA cm⁻² / 1 mA h cm⁻². When assembled with LiFePO₄ cathode, the full cell exhibits an excellent cycle performance (with 71% capacity retention after 4000 cycles) and improved rate performance. The present work provides an effective strategy in forming SEI on 3D electrode host with possible control on the SEI content.

RESULTS AND DISCUSSION

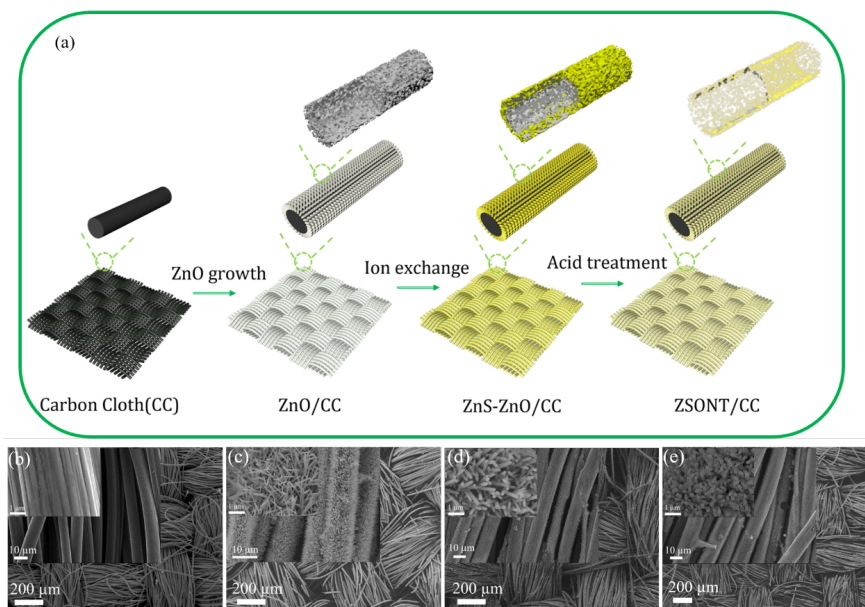


Figure 1. (a) Schematic diagram of fabrication route of ZnS-ZnO nanotubes/carbon cloth (ZSONT/CC). SEM images of (b) carbon cloth (CC), (c) ZnO nanorods on carbon cloth (ZnO/CC), (d) ZnS@ZnO nanocables on carbon cloth (ZnS-ZnO/CC), and (e) ZSONT/CC.

The synthesis process of ZnS-ZnO nanotubes/Carbon Cloth (ZSONT/CC) was illustrated in **Figure 1a**. We first introduced ZnO nanoarrays on the surface of carbon cloth, then formed ZnS-ZnO nanoarrays/Carbon Cloth by ion-exchange method, the following acid treatment led to the formation of the final

product ZSONT/CC. The resulted carbon cloth was found to be similar to its starting counterpart in SEM at low magnification (**Fig. 1b-e**). However, at higher magnifications, the surface of each of carbon fiber (in the cloth) appears modified with one-dimensional nanostructures. **Figure 1c, 1d, and 1e** disclosed the morphological evolution from ZnO/CC, to ZnS-ZnO/CC and to ZnS-ZnO nanotubes (ZSONT)/CC. From the scanning electron microscopy (SEM) image of ZnO/CC (**Fig. 1c**), dense nanoarrays were found on the carbon cloth and the diameter of the individual nanorods is ~ 100 nm. The introduction of ZnS to ZnO/CC led to little change in nanorods' morphology, but the diameter of the NRs increased to ~ 150 nm (**Fig. 1d**). The acid treatment resulted in a tubular structure with a diameter of ~ 150 nm (**Fig. 1e**). As can be seen from the moderately magnified images of ZnO/CC and ZnS-ZnO/CC, they uniformly grew on the entire carbon fiber.

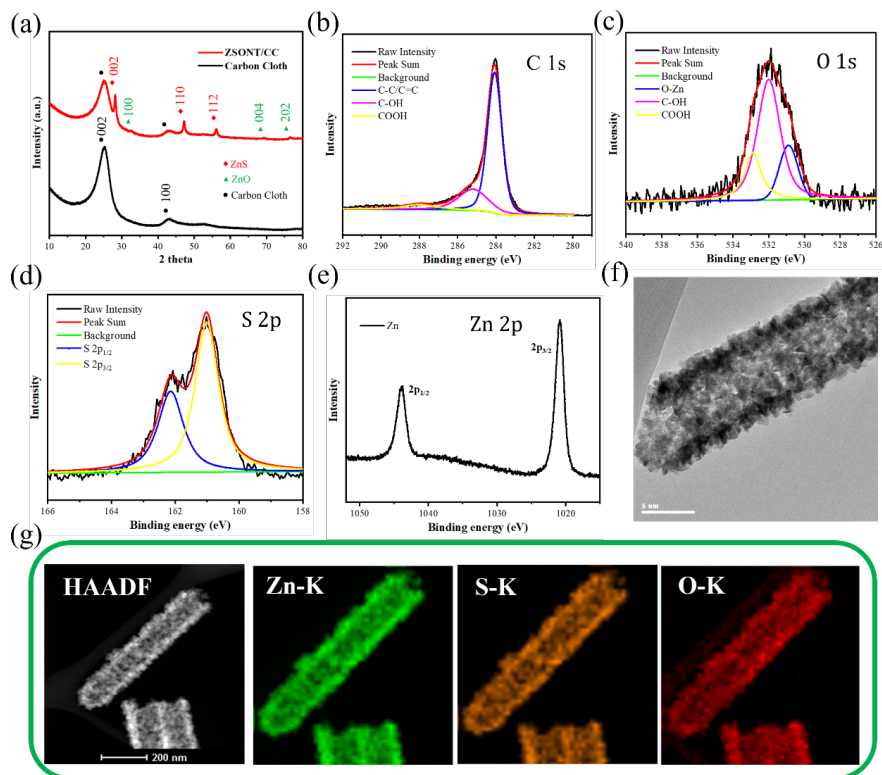


Figure 2. (a) XRD pattern of the ZSONT/CC and carbon cloth. XPS spectra of ZSONT/CC (b) C 1s, (c) O 1s, (d) S 2p, and (e) Zn 2p. (f) TEM image of ZSONT. (g) HAADF-STEM image and the corresponding EDS maps of ZSONT.

The phase of the final product ZSONT/CC and the naked carbon cloth was determined by X-ray diffraction (XRD) (**Fig. 2a**). The peaks located at 25.1° and 43° were the typical peaks of carbon cloth.^[36] Several sharp peaks appeared at 28.2° , 47.2° , and 56.1° , being characteristic of the ZnS diffraction.^[37] Another three small peaks at 32.5° , 69.2° , and 76.6° can be assigned to ZnO, suggesting the co-existence of ZnS and ZnO in the 3D current collector^[38]. X-ray photoelectron spectroscopy (XPS) was exploited to disclose the chemical composition and the chemical bonding property of the ZOSNT/CC, From the XPS survey scan (**Fig. S1**), peaks of Zn, O, C, and S were identified. A fine scan of these compositional elements can be found in **Figure 2b-e**. The carbon 1s located at 284.1, 285.2, and 288 eV could correspond to the C-C/C=C, C-OH, and COOH (**Fig. 2b**). As shown in the O 1s spectrum (**Fig. 2c**), The peak located at 530.8 eV can be assigned to O-Zn, being consistent with XRD results. The other two peaks were associated with C-OH and COOH, likely introduced in the process of acid-treatment of carbon cloth. **Figure 2d** depicted the S 2p

peaks centered at 161.0 and 162.1 eV, which can be ascribed to S 2p_{3/2} and S 2p_{1/2} of ZnS.^[39,40] **Figure 2e** showed the Zn 2p, for which two peaks at 1020.9 and 1043.9 eV can be attributed to the Zn 2p_{3/2} and Zn 2p_{1/2} of ZnS and/or ZnO (the chemical shifts of Zn-O and Zn-S are too small to be distinguished). The tubular structure of ZSONT was recorded by transmission electron microscopy (TEM) (**Fig. 2f**). **Figure 2g** showed the HAADF image of individual nanotubes and EDS mapping of Zn, S, and O. Taken from such a sample, only Zn, S, and O were found in the EDS spectra, and they were uniformly distributed in the entire nanotube. Quantitative composition results of a typical ZSONT sample were shown in **Figure S2**, in which one can find that the Zn (38.84 at. %) and the S (33.50 at. %) are the major components, and the amount of O is low (7.76 at. %). This result suggested that most of O in the original structure of ZnO was replaced by S (The copper signal came from the TEM grid).

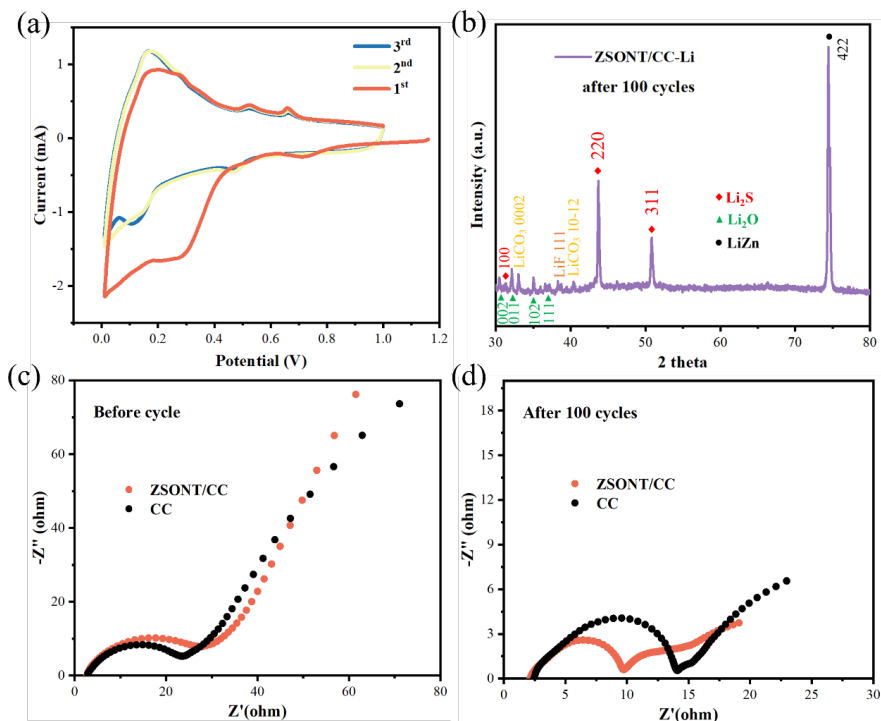
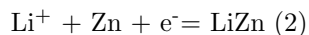
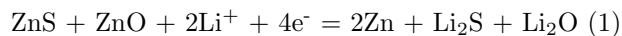


Figure 3 (a) Cyclic Voltammetry (CV) curves of ZSONT/CC electrode in the first three cycles. (b) XRD pattern of ZSONT/CC electrode after 100 cycles. Nyquist plots of Li/ZSONT/CC and Li/CC symmetric cells (c) before cycle and (d) after 100 cycles.

Cyclic voltammetry (CV) analysis of the ZSONT/CC sample was performed in the potential range of 0.01 to 1.0 V (the set potential range was also used in the pre-lithiation process) to see the redox reaction when applied ZSONT/CC and CC hosts. **Figure 3a** showed its CV plots of the first three cycles. The first cathodic peak at 0.7 V can be assigned to the lithiation of ZnS and ZnO that leads to the formation of Li₂S, Li₂O, and Zn metal, and the small peak at ~0.5 V can be attributed to the formation of Li-Zn alloys, with respective reactions shown in eqs 1 and 2.^[41,42]



A broad peak in 0.2-0.4 V can be ascribed to the generation of the solid-electrolyte interface layer and the decomposition of the electrolyte.^[43] In the following anodic sweep, three oxidation peaks located at 0.25, 0.54, and 0.69 V were observed, corresponding to the multistep delithiation process of Li-Zn alloy to metal

Zn. As the potential cut-off is set at 1 V, the oxidation of $\text{Li}_2\text{S} / \text{Li}_2\text{O}$ back to ZnS / ZnO (with oxidation potential ~ 1.26 V) did not occur, and hence in the subsequent cycles, only redox peaks related to Li-Zn were present. The CV results showed that the Li_2S and Li_2O were formed in the pre-lithiation process, and the Zn formed in the cathodic process functioned as lithiophilic sites in the following cycles. XRD of the ZSONT/CC samples after being washed by EC: DEC electrolyte was conducted after they were cycled for 100 runs and lithiated (to 0.05 V). From **Figure 3b**, the peak located at the 30.1° , 32.3° , 34.9° , and 36.8° can be ascribed to the 002, 011, 102, and 111 reflections of Li_2O . The peak at 74.9° is the 422 reflections of LiZn . The two peaks at 44.1° and 51.2° were attributed to the Li_2S . The left three peaks located at 33.0° , 40.4° , and 38.3° came from Li_2CO_3 (0002 and 1012) and LiF (111). The results suggested the persistence of Li_2O and Li_2S in the sample after cycling, in addition to LiZn , Li_2CO_3 , and LiF , with the latter two commonly found in SEI of Li metal electrodes. [44]

Electrochemical impedance spectroscopy tests of Li/ZSONT/CC symmetric cells were carried out to elucidate the fast ion transport kinetics and stable electrolyte-anode interface. Nyquist plots of Li/ZSONT/CC and Li/CC were displayed in **Figure 3**. The fitted results were listed in Table S1 (R_{SEI} : SEI resistance, R_{ct} : charge-transfer resistance, R_1 : internal resistance). From **Figure 3c**, the Li/ZSONT/CC and Li/CC composite anodes have similar interfacial resistance (26.92 and 24.80, respectively) before cycling. After 100 cycles, the R_{SEI} of two electrodes dropped and the R_{ct} of the Li/ZSONT/CC and Li/CC decreased to 4.03 and 2.20 (**Fig. 3d**). Such a reduced resistance is commonly generated by the SEI self-optimizing upon cycling. [45,46] A more significant reduction in R_{SEI} was observed in the Li/ZSONT/CC composite anode (from 26.92 to 8.55) than that of the Li/CC composite anode (from 24.80 to 14.48).

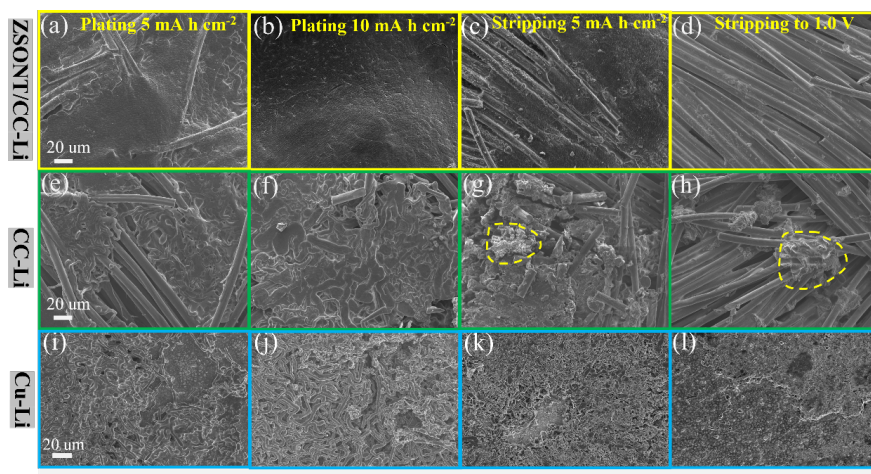


Figure 4. SEM images of morphology evolution of ZSONT/CC electrode, CC electrode, and Cu electrode during the initial cycle: After being plated with Li of (a, e, i) 5 mA h cm^{-2} and (b, f, j) 10 mA h cm^{-2} ; after the anode were stripped (c, g, k) 5 mA h cm^{-2} and (d, h, l) $\sim 10 \text{ mA h cm}^{-2}$ Li from the ZSONT/CC, CC, and Cu electrode.

The lithium plating/stripping behavior on ZSONT/CC host was inspected by a two-electrode cell configuration. Changes in the morphology of the electrodes were observed (**Fig. 4**). When depositing 5 mA h cm^{-2} Li in the ZSONT/CC host (**Fig. 4a**), the empty space in the CC network was almost covered and the porous structure started to disappear. When the deposition capacity of Li increases to 10 mA h cm^{-2} (**Fig.4b**), the carbon fibers were no longer visible (buried) with a flat surface (and dendrite-like features were not observed when compared to the CC electrode and Cu electrode (**Fig. 4e, 4f, 4i, and 4j**)). **Figure S3a** showed that the lithium can be observed from the backside of the electrode, suggesting that the deposition of the lithium was through the entire three-dimensional network of ZSONT/CC, instead of

located on the top surface. A cross-section image of the Li-plated ZSONT/CC was taken (**Fig. S3b**), and a rather uniform lithium distribution was also found. After the anodes were plated with 10 mA h cm^{-2} Li, the stripping process took place, and the lithium started to be removed from the 3D electrode. As the lithium was continuously stripped off the anode, the reverse morphological change was observed, and ZSONT/CC host (fiber-like morphology) appears again (**Fig. 4c and 4d**). In contrast, large lithium patches were observed on the Cu substrate when stripped to 1.0 V (**Fig.4l**), indicating incomplete stripping and thus low coulombic efficiency. The morphology evolution of the CC electrode upon charging and discharging was also investigated. From **Figure 4e**, large chunks were observed on the electrode surface when 5 mA h cm^{-2} lithium was plated. When the plated lithium capacity was increased to 10 mA h cm^{-2} , the surface remained bumpy (**Fig. 4f**). After stripping (**Fig. 4g and 4h**), large patch-like morphology was visible (marked by circles).

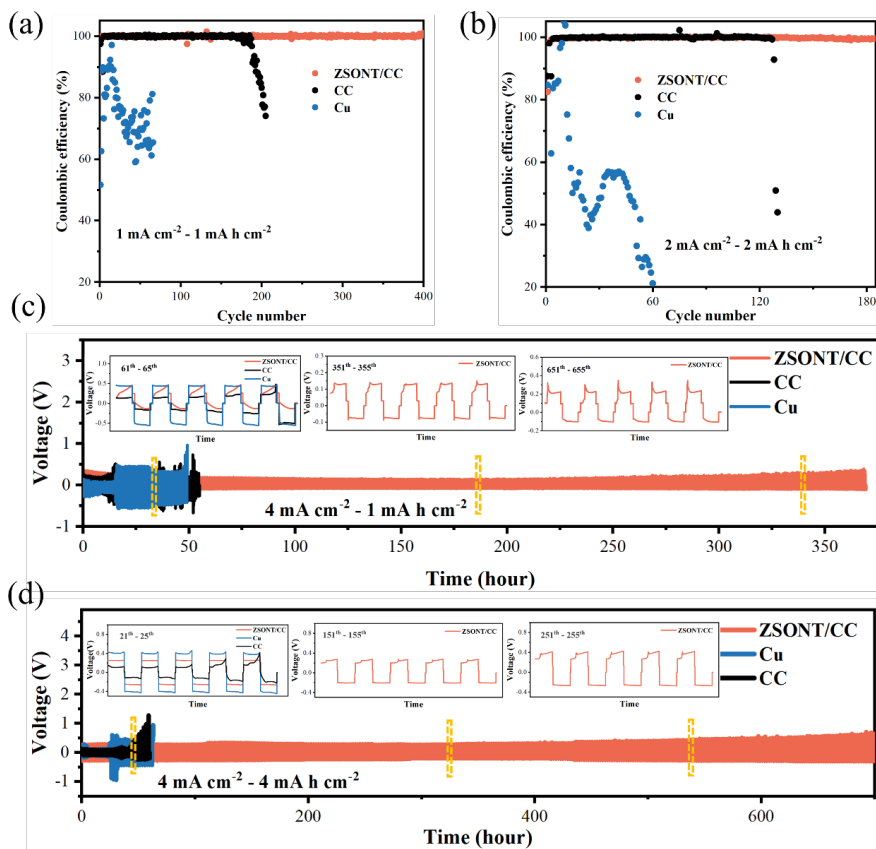


Figure 5. Coulombic efficiencies (CE) of ZSONT/CC//Li, CC//Li, and Cu//Li cells at (a) $1 \text{ mA cm}^{-2} / 1 \text{ mA h cm}^{-2}$ and at (b) $2 \text{ mA cm}^{-2} / 2 \text{ mA h cm}^{-2}$. Galvanostatic cycling performance of Li/ZSONT/CC, Li/CC, and Li/Cu symmetric cells at (c) $4 \text{ mA cm}^{-2} / 1 \text{ mA h cm}^{-2}$ (The inset images are the corresponding enlarged curves of the 61-65th, 351-355th, and 651-655th cycles) and at (d) $4 \text{ mA cm}^{-2} / 4 \text{ mA h cm}^{-2}$ (The inset images are corresponding enlarged curves of the 21-25th, 151-155th, and 251-255th cycles)

Coulombic efficiencies (CE) were tested in ZSONT/CC//Li, CC//Li, and Cu//Li batteries with lithium foil as the counter electrodes in ether electrolyte. The CE value was estimated as the ratio of stripped Li capacity to plated capacity. **Figure 5a** showed the CE comparison of Li on ZSONT/CC host, CC host, and Cu foil at $1 \text{ mA cm}^{-2} / 1 \text{ mA h cm}^{-2}$. The ZSONT/CC electrodes exhibited a stable CE of $\sim 99.2\%$ over 400 cycles. By contrast, the CE of Cu foil fluctuated drastically with a CE below 80.4% in 50 cycles and

the CE of the CC host decreased to 74.3% after 205 cycles. When the current density and capacity were respectively increased to 2 mA cm^{-2} and 2 mA h cm^{-2} , the average CE of the ZSONT/CC was over 99.0% in 180 cycles, whereas that of the Cu foil was below 60.1% in 50 cycles and the CE of the CC host dropped to 43.9% after 130 cycles (**Fig. 5b**). The average CE of ZSONT/CC was found to $>99\%$ in 150 cycles even at $4 \text{ mA cm}^{-2}/1 \text{ mA h cm}^{-2}$, which is much better than CC host (97.2% in 116 cycles) and Cu foil (76.8% in 60 cycles) (**Fig. S4**). The lithiophilic property of the as-prepared ZSONT/CC was accessed by measuring the nucleation overpotentials, taking the Li as the anode and the hosting electrodes as the cathodes. The nucleation overpotential was estimated as $\sim 10.6 \text{ mV}$ for ZSONT/CC electrode, while that of Cu was 325.7 mV (**Fig. S5**). **Figure S6** showed the rate performance of the ZSONT/CC, CC and Cu host at different current densities ranging from 1 to 10 mA cm^{-2} with a fixed capacity of 1 mA h cm^{-2} in symmetrical cells. It was noted that the overpotential was small and steady for ZSONT/CC-Li electrode, specifically, a small voltage hysteresis of 46.7 mV was observed at a current density of 1 mA cm^{-2} . A relatively low overpotential of 263.6 mV was obtained, even at 10 mA cm^{-2} . In contrast, the overpotential of CC was 333.6 mV and that of Cu was 534.2 mV at 10 mA cm^{-2} . These results suggested superior Li ion transport kinetics using the ZSONT/CC-Li electrode. We further compared the cycling stability of the electrodes at small and large capacities. The ZSONT/CC host exhibited stable performance over 650 cycles at $4 \text{ mA cm}^{-2}/1 \text{ mA h cm}^{-2}$ in a symmetrical cell, while CC host only had a life span of ~ 100 cycles and the cell with Cu foil only ran ~ 90 cycles (**Fig. 5c**). At an even higher capacity of 4 mA h cm^{-2} , the symmetrical battery ran stably near 320 cycles (**Fig 5d**), while the cell with CC only lasted for 25 cycles and with Cu lasted for ~ 13 cycles.

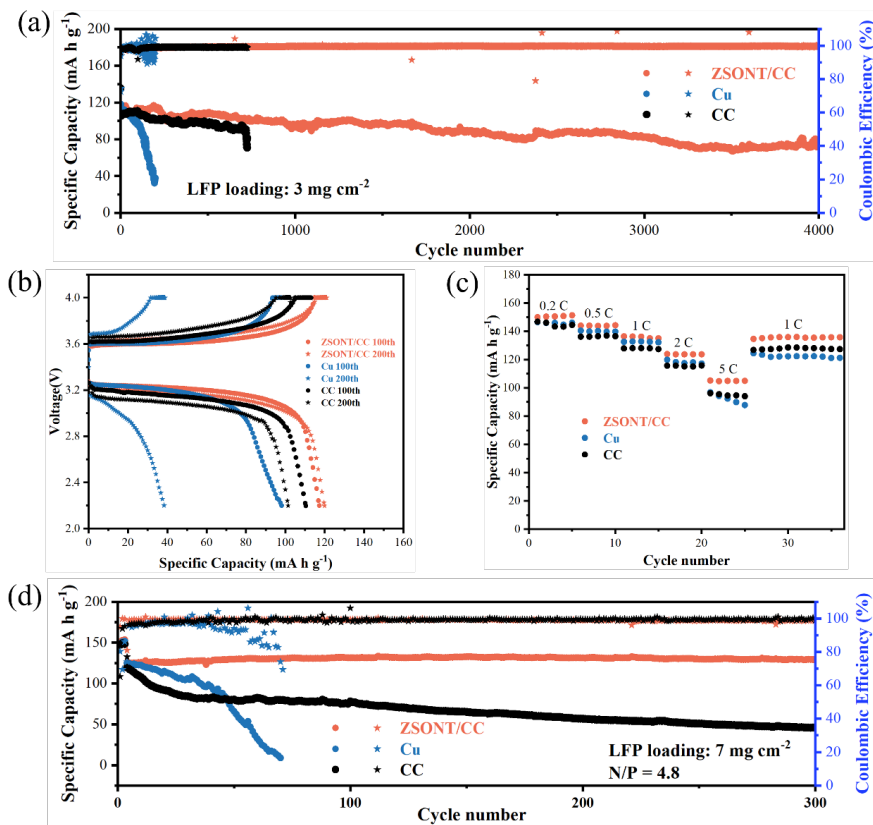


Figure 6. (a) Cycling performance of Li/ZSONT/CC//LiFePO₄(LFP), Li/Cu//LFP, and Li/CC//LFP cells at 2C. (b) Charging/discharging curves of Li/ZSONT/CC//LFP, Li/Cu//LFP and Li/CC//LFP cells in the 100th and 200th cycle. (c) Rate performance of Li/ZSONT/CC//LFP, Li/Cu//LFP and Li/CC//LFP batteries cycled from 0.2 to 5C. (d) Cycling performance of high-loading Li/ZSONT/CC//LFP, Li/Cu//LFP

and Li/CC//LFP batteries at 2C (cathode loading=7.0mg cm⁻², N: P=4.8).

To demonstrate the practical application of ZSONT/CC host, Li/ZSONT/CC//LiFePO₄ (LFP) cells (with 4 mA h cm⁻² Li) were assembled using ester-based electrolyte. For comparison, Li/Cu//LFP and Li/CC//LFP full cells were also assembled with the same parameters. As depicted in **Figure 6a**, Li/ZSONT/CC//LFP cell delivered excellent cycle stability with retaining capacity up to 77 mA h g⁻¹ (with a capacity retention of 71%) after 4000 cycles at 2C, exhibiting a high average CE of 99.2%. In contrast, Li/Cu//LFP cell showed a fast capacity degradation and a low-capacity retention of 33.2% after 200 cycles, and Li/CC//LFP cell dropped to 71 mA h g⁻¹ after 725 cycles (with a capacity retention of 66.5%). **Figure 6b** showed the charge/discharge curves of two full cells in the 100th cycle and 200th cycle. Although the voltage plateau gap of the three cells was similar in the 100th cycle, a much smaller polarization voltage was observed in Li/ZSONT/CC//LFP full cell after 200 cycles. Besides, Li/ZSONT/CC//LFP full cell exhibited a superior rate performance to the other two (**Fig. 6c**), especially at large rates, the specific capacities of Li/ZSONT/CC//LFP full cell can reach up to 104.9 mA h g⁻¹ at 5C, much better than Li/Cu//LFP (92.3 mA h g⁻¹ at 5C) and Li/CC//LFP (95.4 mA h g⁻¹ at 5C). Moreover, an N/P ratio of 4.8 with 7mg cm⁻² LFP was chosen for the full cell that was cycled (**Fig. 6d**) at a charging/discharging rate of 2C. The cell can run for over 300 cycles with little capacity decay, demonstrating excellent cycling performance. As a comparison, Li/Cu//LFP full cell showed a lifespan of 70 cycles, and the capacity of Li/CC//LFP full cell faded to 45.8 mA h g⁻¹ at the end of 300 cycles.

CONCLUSIONS

In summary, an advanced 3D skeleton (ZSONT/CC) was developed to serve as lithium metal host with both structural and compositional homogeneity for high-performance LMBs. Upon lithiation, the in-situ formed Li₂S-Li₂O-LiZn rich SEI on 3D carbon host efficiently guided the uniform lithium deposition, stabilized the electrolyte-electrode interface, and facilitated Li⁺ ion transport in the repeating lithium plating/stripping process. As a result, excellent cycle stability was maintained when Li/ZSONT/CC anode was applied in symmetrical cells and full cells, and a high CE was achieved. This work provides an effective design strategy for SEI formation on a 3D electrode host with possible control on the SEI content.

ACKNOWLEDGMENTS

The authors acknowledge the funding support of CUHK Direct grant, under Project No. 4053413.

CONFLICT OF INTEREST

The authors declare no conflict of interest.

ORCID

Quan Li <https://orcid.org/0000-0001-8563-1802>

Experimental section

The pre-treatment of carbon cloth: The carbon cloth was immersed in 4M H₂SO₄ for 12 hours and then washed by DIW several times, eventually treated at 400 for 1 h. The carbon cloth was punched into small disks with an area of about 1 cm⁻² by a punching machine.

A similar synthesis process of ZSONT/CC is reported,^[47] here listed for convenience. Firstly, ZnO seeds were introduced by immersing carbon cloth disks in zinc acetate dihydrate/ethanol solution three times, followed by vacuum filtration and drying in a Muffle furnace at 350 . The ZnO nanorods were obtained by hydrothermal treatment (immersing the ZnO seeds decorated carbon cloth into aqueous solution containing zinc nitrate hexahydrate (25mM) and methenamine (25mM) at 95 for 6 h), followed by washing several times with DIW and vacuum drying at 60 . The ZnS/ZnO/carbon cloth was obtained by immersing the ZnO nanorods decorated carbon cloth into 30 ml aqueous solution containing 0.4 M sodium sulfide and 100 μ l thioglycolic acid in a water bath at 60 for 4h, followed by vacuum drying at 60. The ZSONT/CC was

obtained by immersing the ZnS/ZnO/carbon cloth into 5wt.% acetic acid solution for 30 minutes, followed by vacuum drying at 60.

Characterization : JEOL JSM-7800F field emission was exploited to record the morphology features of the samples. X-ray diffraction measurements were performed using a SmartLab, Rigaku with a Cu-K α radiation source ($\lambda=0.1541\text{nm}$). A Tecnai F20 ST(FEI) microscope was used to record the TEM image. Energy-dispersive X-ray spectroscopy (EDS) was used to take element mapping. XPS measurements were carried out using a spectrometer ((Nicolet NEXUS-670) Thermo Scientific, USA)).

Electrochemical measurement : 2032 type coin cells were used to evaluate electrochemical performance in an Argon gas filling glove box ($\text{H}_2\text{O} < 0.5 \text{ ppm}$, $\text{O}_2 < 0.5 \text{ ppm}$). The obtained ZSONT/CC host, CC host and Cu were used as working electrodes. Ether Electrolyte was composed of 1M Lithium bis (trifluoromethanesulfonyl) imide (LiTFSI) in 1,3 dioxolane/1,2-dimethoxyethane (DOL/DME, V/V = 1/1) electrolyte with 1 wt.% LiNO_3 as additives while carbonate electrolyte consisted of 1M Lithium hexafluorophosphate (LiPF_6) in ethylene carbonate/diethyl carbonate (EC/DEC, V/V = 1/1) electrolyte. The separator is Celgard 3501. A battery testing system (LAND battery tester, Wuhan, China) was exploited to test battery performance. To study the depositing/stripping behavior of the host, the cells were disassembled after reaching the corresponding states. To eliminate the dirties, cells were run between 0.01V - 1.0 V (vs. Li/Li^+) for three cycles, then 4 mA h cm^{-2} Li was deposited on the ZSONT/CC, CC and Cu host. LiFePO_4 was selected as the cathode to assemble full cells and Li/ZSONT/CC, Li/CC and Li/Cu were chosen as anodes. The mass loading of the LFP cathode is 3.0 mg cm^{-2} and 7.0 mg cm^{-2} . The amount of electrolyte is 80 μl and 60 μl in the symmetric cells and full cells, respectively. The Coulombic efficiency was tested in Li//ZSONT/CC, Li//CC, and Li//Cu cells in ether electrolyte. LiFePO_4 electrode was composed of active materials (80 wt.%), polyvinylidene difluorides (PVDF) binder (10 wt.%), and carbon black (10 wt.%), the cathode was spread on an aluminum foil. Cyclic voltammetry (CV) scanned at a sweep rate of 0.05 mV/s and electrochemical impedance spectroscopy (EIS) performed in the frequency between 100 kHz and 0.01Hz were measured on a CHI770C electrochemical workstation (Chen Hua Instrument Co., China).

REFERENCES

1. Lin D, Liu Y, Cui Y, Reviving the lithium metal anode for high-energy batteries. *Nat. Nanotechnol.* 2017;12;194-206.
2. Cheng XB, Zhang R, Zhao CZ, Zhang Q, Toward safe lithium metal anode in rechargeable batteries: a review. *Chem Rev.* 2017;117;10403-10473.
3. Jin C, Sheng O, Luo J, Yuan H, Fang C, Zhang W, Hui H, Gan Y, Xia Y, Liang C, Zhang J, Tao X. 3D lithium metal embedded within lithiophilic porous matrix for stable lithium metal batteries. *Nano Energy.* 2017;37;177-186.
4. Jana A, Woo SI, Vikrant KSN, García RE, Electrochemomechanics of lithium dendrite growth. *Energy Environ Sci.* 2019;12;3595-3607.
5. Xiao J, Li Q, Bi Y, Cai M, Dunn B, Glossmann T, Liu J, Osaka T, Sugiura R, Wu B, Yang J, Zhang JG, Whittingham MS, Understanding and applying coulombic efficiency in lithium metal batteries. *Nat Energy.* 2020;5;561-568.
6. Ghazi ZA, Sun Z, Sun C, Qi F, An B, Li F, Cheng HM, Key aspects of lithium metal anodes for lithium metal batteries. *Small.* 2019;15;1900687.
7. Tikekar MD, Choudhury S, Tu Z, Archer LA, Design principles for electrolytes and interfaces for stable lithium-metal batteries. *Nat Energy.* 2016;1;1-7.
8. Zhai P, Liu L, Gu X, Wang T, Gong Y, Interface engineering for lithium metal anodes in liquid electrolyte. *Adv Energy Mater.* 2020;10;2001257.
9. Zhang H, Eshetu GG, Judez X, Li C, Rodriguez-Martinez LM, Armand M, Electrolyte additives for

lithium metal anodes and rechargeable lithium metal batteries: progress and perspectives. *Angew Chem Int Ed* . 2018;57;15002-15027.

10. Xu R, Zhang XQ, Cheng XB., Peng HJ, Zhao CZ, Yan C, Huang JQ, Artificial soft-rigid protective layer for dendrite-free lithium metal anode. *Adv Funct Mater* . 2018;28;1705838.

11. Lee H, Lee DJ, Kim YJ, Park JK, Kim HT, A simple composite protective layer coating that enhances the cycling stability of lithium metal batteries. *J Power Sources* . 2015;284;103-108.

12. Simon FJ, Hanauer M, Richter FH, Janek J, Interphase formation of PEO20: LiTFSI-Li₆PS₅Cl composite electrolytes with lithium metal. *ACS Appl Mater Interfaces* . 2020;12;11713-11723.

13. Park S, Jin HJ, Yun YS. Advances in the design of 3D-structured electrode materials for lithium-metal anodes. *Adv Mater* . 2020;32;2002193.

14. Shen F, Zhang F, Zheng Y, Fan Z, Li Z, Sun Z, Xuan Y, Zhao B, Lin Z, Gui X, Han X, Cheng Y, Niu C. Direct growth of 3D host on Cu foil for stable lithium metal anode. *Energy Storage Mater* . 2018;13;323-328.

15. Jiang Z, Jin L, Zeng Z, Xie J. Facile preparation of a stable 3D host for lithium metal anodes. *Chem Commun* . 2020;56;9898-9900.

16. Le T, Yang C, Liang Q, Huang X, Kang F, Yang Y. A fishing-net-like 3D host for robust and ultrahigh-rate lithium metal anodes. *Small* . 2021;17;2007231.

17. Wang JP, Lan DN, Chen GY, Hu XT, Lin C, Li Q. Built-in stable lithiophilic sites in 3D current collectors for dendrite free Li metal electrode. *Small* . 2022;18;2106718.

18. Xia Y, Jiang Y, Qi Y, Zhang W, Wang Y, Wang S, Liu Y, Sun WX. Zhao Z. 3D stable hosts with controllable lithiophilic architectures for high-rate and high-capacity lithium metal anodes. *J Power Sources* . 2019;442;227214.

19. Li Q, Zhu S, Lu Y. 3D porous Cu current collector/Li-metal composite anode for stable lithium-metal batteries. *Adv Funct Mater* . 2017;27;1606422.

20. Zhang K, Wu F, Zhang K, Weng S, Wang X, Gao M, Sun Y, Cao D, Bai Y, Xu H, Wang X, Wu C. Chlorinated dual-protective layers as interfacial stabilizer for dendrite-free lithium metal anode. *Energy Storage Mater* . 2021;41;485-494.

21. Jung S, Brown ZL, Kim J, Lucht BL. Effect of electrolyte on the nanostructure of the solid electrolyte interphase (SEI) and performance of lithium metal anodes. *Energy Environ Sci* . 2018;11;2600-2608.

22. Cheng XB, Zhang R, Zhao CZ, Wei F, Zhang JG, Zhang Q. A review of solid electrolyte interphases on lithium metal anode. *Adv Sci* . 2016;3;1500213.

23. Liu F, Wang L, Zhang Z, Shi P, Feng Y, Yao Y, Ye S, Wang H, Wu X, Yu Y. A mixed lithium-ion conductive Li₂S/Li₂Se protection layer for stable lithium metal anode. *Adv Funct Mater* . 2020;30;2001607.

24. Sun S, Myung S, Kim G, Lee D, Son H, Jang M, Park E, Son B, Jung YG, Park U, Song T. Facile ex situ formation of a LiF-polymer composite layer as an artificial SEI layer on Li metal by simple roll-press processing for carbonate electrolyte-based Li metal batteries. *J Mater Chem A* . 2020; 8;17229-17237.

25. Hu A, Chen W, Du X, Hu Y, Lei T, Wang H, Xue L, Li Y, Sun H, Yan Y, Long J, Shu C, Zhu J, Li B, Wang X, Xiong J. An artificial hybrid interphase for an ultrahigh-rate and practical lithium metal anode. *Energy Environ Sci* . 2021;14; 4115-4124.

26. Zhai P, Wang T, Jiang H, Wan J, Wei Y, Wang L, Liu W, Chen Q, Yang W, Cui Y, Gong Y. 3D artificial solid-electrolyte interphase for lithium metal anodes enabled by insulator-metal-insulator layered heterostructures. *Adv Mater* . 2021;33;2006247.

27. Liu P, Su H, Liu Y, Zhong Y, Xian C, Zhang Y, Wang X, Xia X, Tu J. LiBr–LiF-rich solid–electrolyte interface layer on lithiophilic 3D framework for enhanced lithium metal anode. *Small Struct* . 2022, 3, 2200010.
28. Li K, Hu Z, Ma J, Chen S, Mu D, Zhang J, A 3D and stable lithium anode for high-performance lithium-iodine batteries, *Adv. Mater* . 2019;31;1902399.
29. Meng JK, Wang WW, Yue XY, Xia HY, Wang QC, Wang XX, Fu ZW, Wu XJ, Zhou YN, Cotton-derived carbon cloth enabling dendrite-free Li deposition for lithium metal batteries, *J. Power Sources* . 2020;465;228291.
30. Deng W, Zhu WH, Zhou XF, Peng XQ, Liu ZP, Highly reversible li plating confined in three-dimensional interconnected microchannels toward high-rate and stable metallic lithium anodes, *ACS Appl Mater Interfaces* . 2018;10;20387–20395.
31. You L, Ju S, Liu J, Xia G, Guo Z, Yu X, Synergistic effect of lithiophilic Zn nanoparticles and N-doping for stable Li metal anodes, *J Energy Chem* . 2022;65;439-447.
32. Cao J, Xie Y, Yang Y, Wang X, Li W, Zhang Q, Ma S, Cheng S, Lu B, Achieving uniform Li plating/stripping at ultrahigh currents and capacities by optimizing 3D nucleation Sites and Li₂Se-Enriched SEI. *Adv Sci* . 2022;9;2104689.
33. Sun C, Li Y, Jin J, Yang J, Wen Z. ZnO nanoarray-modified nickel foam as a lithiophilic skeleton to regulate lithium deposition for lithium-metal batteries. *J Mater Chem A* . 2019;7;7752-7759.
- 34 Han M, Liu G, Jiang J, Lu S, Jiang Y, Liu Y, Zhao B, Zhang J. Realizing spherical lithium deposition by in situ formation of a Li₂S/Li–Sn alloy mixed layer on carbon paper for stable and safe Li metal anodes. *ACS Appl Mater Interfaces* . 2021; 13;48828-48837.
35. Hu W, Yao Y, Huang X, Ju S, Chen Z, Li M, Wu Y. CuO nanofilm-covered Cu microcone coating for a long cycle Li metal anode by in situ formed Li₂O. *ACS Applied Energy Mater* . 2022;5;3773-3782.
36. Huang Z, Zhang Z, Qi X, Ren X, Xu G, Wan P, Sun X, Zhang H. Wall-like hierarchical metal oxide nanosheet arrays grown on carbon cloth for excellent supercapacitor electrodes. *Nanoscale* . 2016;8 ;13273-13279.
37. Zhu J, Zhou M, Xu J, Liao X. Preparation of CdS and ZnS nanoparticles using microwave irradiation. *Mater Lett* . 2001;47 ;25-29.
38. Van Heerden JL, Swanepoel R. XRD analysis of ZnO thin films prepared by spray pyrolysis. *Thin Solid Films* . 1997;299 ;72-77.
39. Lytle JC, Wallace JM, Sassin MB, Barrow AJ, Long JW, Dysart JL, Renninger CH, Saunders MP, Brandell NL, Rolison D R. The right kind of interior for multifunctional electrode architectures: carbon nanofoam papers with aperiodic submicrometre pore networks interconnected in 3D. *Energy Environ Sci*. 2011;4 ;1913-1925.
40. Mao M, Jiang L, Wu L, Zhang M, Wang T. The structure control of ZnS/graphene composites and their excellent properties for lithium-ion batteries. *J Mater Chem A* . 2015;3 ;13384-13389.
41. He L, Liao XZ, Yang K, He YS, Wen W, Ma ZF. Electrochemical characteristics and intercalation mechanism of ZnS/C composite as anode active material for lithium-ion batteries. *Electrochim Acta* . 2011;56 ;1213-1218.
42. Tan L, Li X, Cheng M, Liu T, Wang Z, Guo H, Yan G, Li L, Liu Y, Wang J. In-situ tailored 3D Li₂O@ Cu nanowires array enabling stable lithium metal anode with ultra-high coulombic efficiency. *J Power Sources* . 2020;463 ;228178.

43. Zhang W, Yin J, Lin Z, Lin H, Lu H, Wang Y, Huang W. Facile preparation of 3D hierarchical porous carbon from lignin for the anode material in lithium ion battery with high rate performance. *Electrochim Acta* . 2015; 176 ;1136-1142.
44. Jin C, Liu T, Sheng O, Li M, Liu T, Yuan Y, Nai J, Ju Z., Zhang W., Liu Y, Wang Y, Lin Z, Lu J, Tao X, Rejuvenating dead lithium supply in lithium metal anodes by iodine redox. *Nat Energy* . 2021;6;378-387.
45. Zhang R, Chen X, Shen X, Zhang XQ, Chen XR, Cheng XB, Yan C, Zhao Z, Zhang Q. Coralloid carbon fiber-based composite lithium anode for robust lithium metal batteries. *Joule* . 2018;2 ;764-777.
46. Lu C, Tian M, Zheng X, Wei C, Rummeli MH, Strasser P, Yang R. Cotton pad derived 3D lithiophilic carbon host for robust Li metal anode: In-situ generated ionic conductive Li₃N protective decoration. *Chem Eng J* . 2022; 430 ; 132722.
47. Huang L, Zhang Y, Shang C, Wang X, Zhou G, Ou JZ, Wang Y. ZnS nanotubes/carbon cloth as a reversible and high-capacity anode material for lithium-ion batteries. *ChemElectroChem* . 2019; 6; 461-466.

Supporting information

In situ tailoring solid electrolyte interphase of three-dimensional Li metal electrode for enhanced Coulombic efficiency

Jiang-Peng Wang, Feng Lang, Quan Li*

Department of Physics, the Chinese University of Hong Kong, Shatin, New Territory, China

Corresponding Author

Q. Li: liquan@cuhk.edu.hk

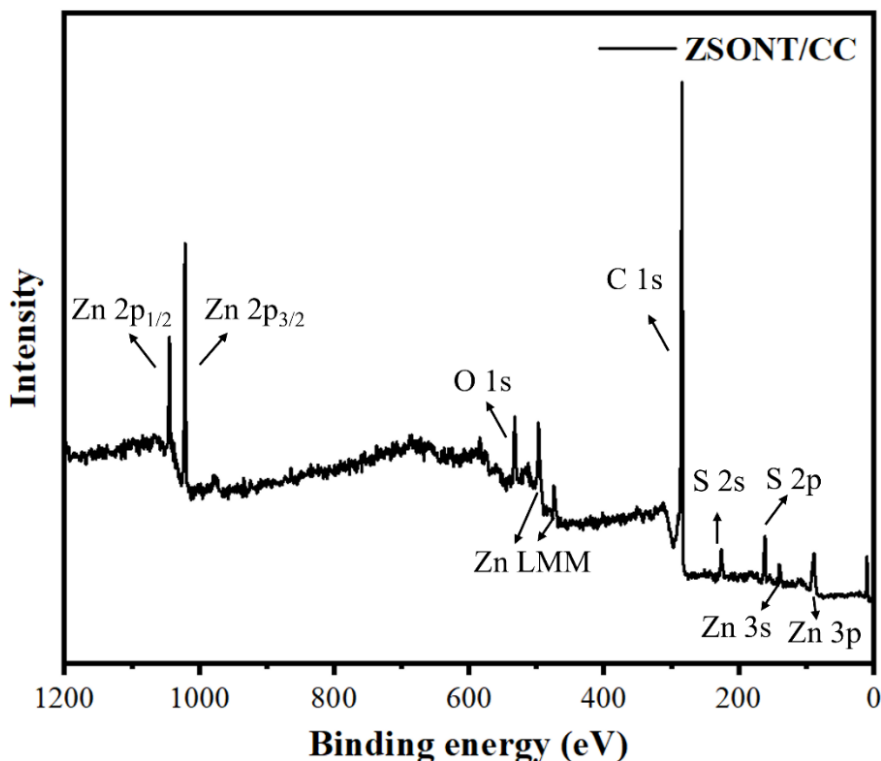


Figure S1. X-ray photoelectron spectroscopy (XPS) survey spectrum of ZSONT/CC. Four obvious elements

could be observed, the X-ray photoelectron spectroscopy survey scan suggests that the ZSONT/CC is mainly composed of C, O, S and Zn.

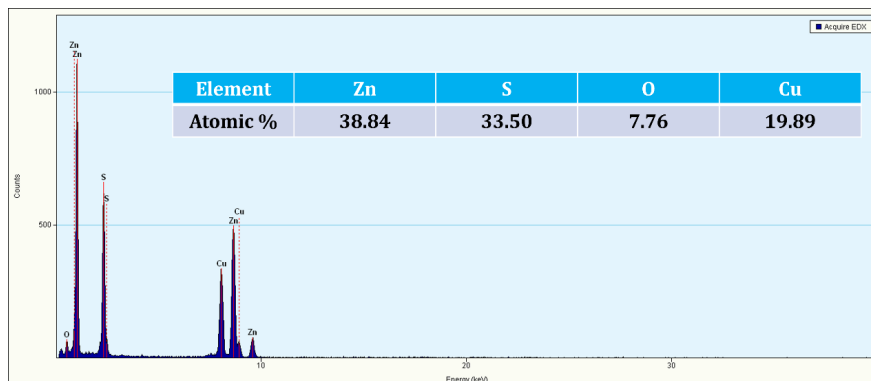


Figure S2. (a) A typical EDS spectrum taken from the ZSONT sample with its composition listed in the inset table.

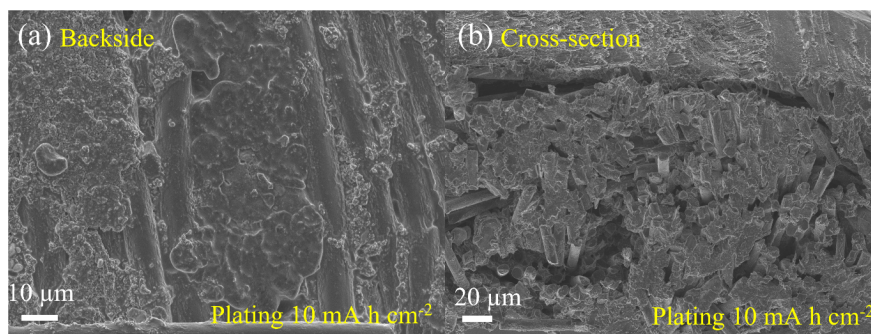


Figure S3. (a) SEM image of the backside of ZSONT/CC-Li after plating 10 mA h cm^{-2} . (b) Cross-section image of ZSONT/CC-Li after 10 mA h cm^{-2} plating.

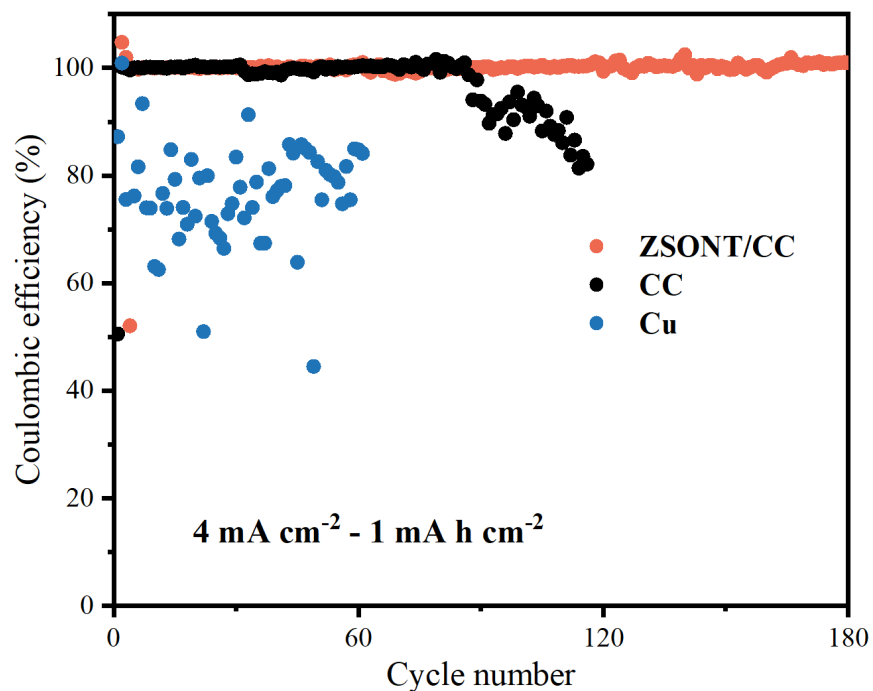


Figure S4. Coulombic efficiencies of the ZSONT/CC and Cu foil electrodes at 4 mA cm⁻² and capacity of 1 mA h cm⁻².

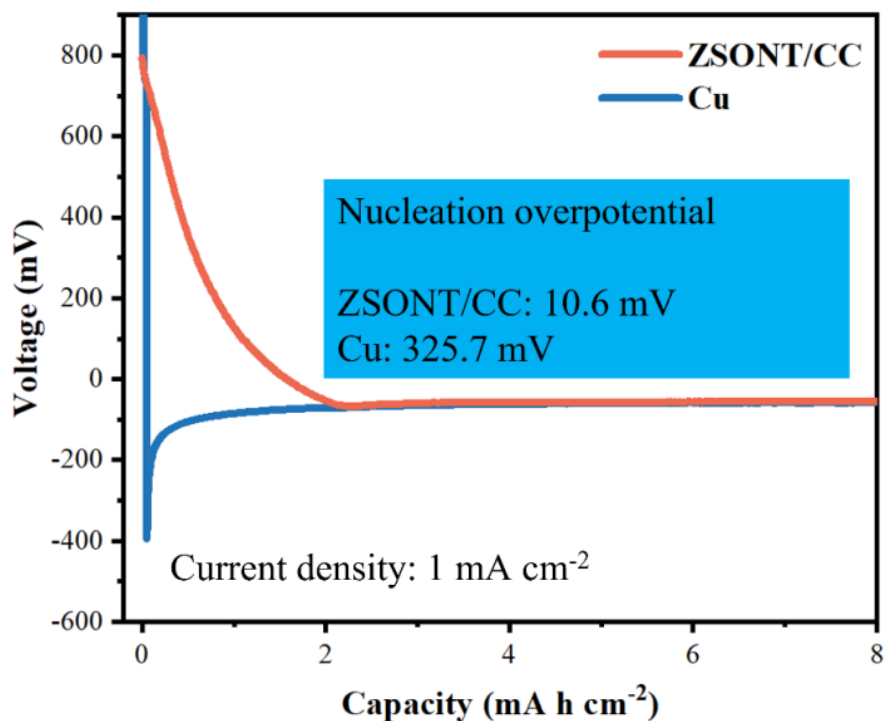


Figure S5. Voltage-areal capacity plots upon Li nucleation at 1 mA cm⁻² with a total Li deposition amount of 8 mA h cm⁻² on the ZSOCC and the Cu electrodes.

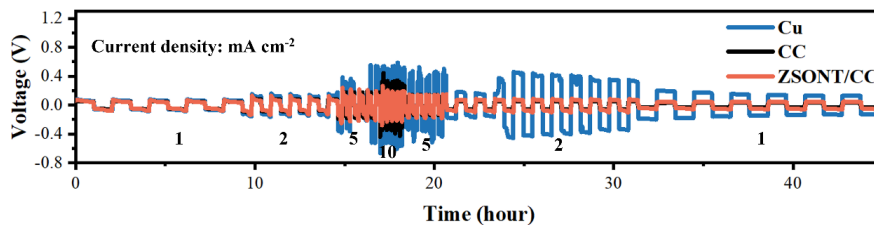


Figure S6. Rate performance of ZSONT/CC-Li, CC-Li, and Cu-Li composite electrodes in their respective symmetric cells at various current densities with a fixed capacity of 1 mA h cm^{-2} .

Table S1. The value of R_1 , R_{SEI} , and R_{ct} of Li symmetrical cells before cycling and after 100 cycles.

| Sample | ZSONT/CC | ZSONT/CC | CC | CC |
|----------------------|----------------|----------|--------------|-------|
| Cycle number | Before cycling | 100th | Before cycle | 100th |
| R_1/Ohm | 2.80 | 2.16 | 2.89 | 2.42 |
| R_{SEI}/Ohm | 26.92 | 8.55 | 24.80 | 14.48 |
| R_{ct}/Ohm | | 4.03 | | 2.20 |

Hosted file

Figures.docx available at <https://authorea.com/users/583522/articles/623103-in-situ-tailoring-solid-electrolyte-interphase-of-three-dimensional-li-metal-electrode-for-enhanced-coulombic-efficiency>